

Aumann-SHAP: The Geometry of Counterfactual Interaction Explanations in Machine Learning

Adam Belahcen¹ and Stéphane Mussard²

¹ AIRESS & UM6P, Morocco adam.belahcen@um6p.ma

² CHROME, Univ. Nîmes; AIRESS & UM6P stephane.mussard@unimes.fr

Abstract. We introduce **Aumann-SHAP**, an interaction-aware framework that decomposes counterfactual transitions by restricting the model to a local hypercube connecting baseline and counterfactual features. Each hyper-cube is decomposed into a grid in order to construct an induced micro-player cooperative game in which elementary grid-step moves become players. Shapley and LES values on this TU-micro-game yield: (i) within-pot contribution of each feature to the interaction with other features (interaction explainability), and (ii) the contribution of each instance and each feature to the counterfactual analysis (individual and global explainability). In particular, Aumann-LES values produce individual and global explanations along the counterfactual transition. Shapley and LES values converge to the diagonal Aumann-Shapley (integrated-gradients) attribution method. Experiments on the German Credit dataset and MNIST data show that Aumann-LES produces robust results and better explanations than the standard Shapley value during the counterfactual transition.

Keywords: Aumann-Shapley · Counterfactuals · Game theory · XAI.

1 Introduction

Machine learning models must be explainable, contestable, and actionable [8], which has motivated the development of explainable artificial intelligence (XAI). A dominant approach to XAI is feature attribution, where given an instance \mathbf{x} and a predictor $g(\cdot)$, the objective is to decompose a score $g(\mathbf{x})$ into feature-wise contributions that satisfy an *efficiency* property (the contributions sum to what is being explained).

The Shapley value [26] provides an axiomatic foundation for such decompositions and underlies widely used tools such as SHAP [20], with applications spanning from human resources analytics to bank performance evaluation [27] among others. Beyond the classical Shapley value, related rules include Aumann-Shapley / Integrated Gradients for path-based settings [2, 32] and interaction-aware indices such as Shapley-Taylor [30]. Different coalition-value definitions yield different explanation semantics [31]. More generally, different modeling choices (*e.g.*, baselines and reference distributions) induce different “Shapley

values for explanation” [31]. Finally, fair and efficient non-Shapley alternatives within the Linear–Efficient–Symmetric (LES) family have also been advocated for attribution [7].

In many applications, however, the core question is not why the model predicted $g(\mathbf{x}^0)$ at a baseline point, but how to change inputs to obtain a desired or feasible outcome $g(\mathbf{x}^1)$. This is the setting of counterfactual explanations and algorithmic recourse [17, 21, 33, 35]. Standard generators include optimization-based formulations [35], randomized search procedures such as DiCE [21], and boundary-search methods like Growing Spheres [17]. While these methods identify which features change between \mathbf{x}^0 and \mathbf{x}^1 , they typically do not quantify how much each changed feature contributed to the improvement, nor do they explain how *interactions* between features drive the transition.³

A natural way to explain counterfactual transitions is to attribute the *difference* $\Delta y := g(\mathbf{x}^1) - g(\mathbf{x}^0)$ via cooperative-game decompositions. Using Harsanyi dividends [12], it is possible to allocate interaction pots between features to each individual feature. The standard Shapley rule splits each pot equally among its members [19], providing a symmetric baseline as a natural starting point for explainability of counterfactual paths. However, equal splitting ignores the geometry of the transition, treating all features symmetrically regardless of whether a feature enables an interaction early by entering a synergistic regime or harvests it only after others shift.

The main contributions are the following:

1. We introduce a micro-player Transferable-utility game (TU-game) for counterfactual transitions by discretizing the local baseline counterfactual hypercube and treating grid-step moves as players.
2. We derive the Aumann-SHAP (micro-game Shapley), an attribution method that yields geometry-aware, within-pot contributions of pure interactions between features (recovering the equal-split Shapley [19] as a special case).
3. We generalize the framework to an Aumann–LES family, enabling robustness comparisons across attribution rules on the same counterfactual change.
4. We provide an exact grid-state closed form that avoids enumerating 2^n micro-coalitions and gives polynomial-time computation in grid resolution (for fixed interaction order).

Section 2 reviews related work on attribution and counterfactual explanations. Section 3 introduces the local-cube residual interactions and the induced micro-game construction. Section 4 presents micro-game-Shapley and Aumann-LES attribution methods and their theoretical properties. Section 5 reports simulations, experiments and robustness analyses on German credit and MNIST data. Section 6 concludes.

³ This gap is especially acute in nonlinear models (*e.g.*, ensembles), where a feature may be weak in isolation but decisive in combination, and where effects can depend on the order/context of changes along the baseline-to-counterfactual transition, motivating path-based interpretability analyses [19]. Related concerns are also emphasized in the recourse literature, as nearest counterfactuals can fail to correspond to actionable interventions [16, 34].

2 State of the art

2.1 Explainability and feature attribution

XAI methods, *i.e.* attribution methods for black-box models, fall into three families, and each one of them can potentially mask *interactions* between features [8]. The first relies on local surrogates that approximate $g(\cdot)$ around an input, as in LIME [23]. A leading approach is Shapley attribution, which treats features as cooperative-game players and derives attributions from coalition values [20, 26]. Shapley methods satisfy axioms such as symmetry and efficiency and work well for tabular data [20, 26], but different definitions of coalition values (*e.g.*, missingness, conditioning, causality) yield different explanations [10, 14, 31]. Alternative rules within the Linear-Efficient-Symmetric (LES) family trade off axioms and computation and allow robustness comparisons [7]. The second family includes gradient and path-based methods for differentiable models [8]. Integrated Gradients (IG) attributes prediction changes along a baseline-to-input path [32] and connects to the continuous Aumann-Shapley value [2]. Vision-oriented saliency methods (*e.g.*, Grad-CAM, SmoothGrad) are common [25, 28], though our focus is on tabular data where interaction accounting is central. The third family uses perturbation and global sensitivity analysis, such as permutation importance, PDP, ICE, ALE, and Sobol indices [1, 4, 9, 11, 29]. While useful for global insight, they do not provide a single local additive decomposition for a baseline-to-target change, nor isolate pure interaction pot features.

2.2 Explainability and counterfactual analysis

Counterfactual explanations address a different question than pointwise attribution: instead of asking why $g(\mathbf{x}^0)$ occurred (*e.g.* why a client is not creditworthy), the goal is to find how inputs should change to reach a desired outcome $g(\mathbf{x}^1)$ (the client becomes creditworthy).

Much of the literature focuses on generating counterfactuals (generators), such as DiCE [21] and boundary-expansion strategies like Growing Spheres [17]. Counterfactuals are typically non-unique: many feasible \mathbf{x}^1 may exist with similar distance but different changed features, so robustness to the generator and its hyperparameters is important when explanations guide actions or compliance narratives. While generators provide what changed between \mathbf{x}^0 and \mathbf{x}^1 , they usually do not quantify how much each change contributed to the shift $g(\mathbf{x}^1) - g(\mathbf{x}^0)$, nor how interactions mediated the shift. This is especially problematic in nonlinear models, where effects are context- and path-dependent, motivating path-based counterfactual explanation [19].

Interaction attribution within counterfactual analysis is essential for non-additive models. A common route is to define a cooperative game using hybrid inputs and decompose the total change into Harsanyi interaction pots [12]. In this context, the Shapley value [26] allocates each pot by equal split among its members, yielding a Shapley-grounded baseline for counterfactual transitions [19, 20]. However, the equal split issued from Shapley [19] is blind to geometry,

it cannot distinguish whether a feature enables an interaction early along the move from \mathbf{x}^0 to \mathbf{x}^1 or harvests it later after other coordinates have changed.

Our contribution targets this interface between the geometry of counterfactual paths and attribution methods. For each counterfactual transition, we restrict the model to the local hypercube connecting $(\mathbf{x}^0, \mathbf{x}^1)$, isolate pure interaction structure *via* inclusion–exclusion, and discretize the cube to induce a micro-player game. This yields a geometry-aware redistribution of interaction pots that remains efficient and supports robustness checks through LES alternatives [7].

3 TU-micro-game: decomposition of feature interactions

3.1 Setup

Notation. Fix $d \geq 2$ and let $N := \{1, \dots, d\}$ index the features. A coalition is any subset $S \subseteq N$. Let $g : \mathcal{X} \rightarrow \mathbb{R}$ be a predictive functional on an input space $\mathcal{X} \subseteq \mathbb{R}^d$, and let $\mathbf{x} = (x_1, \dots, x_d) \in \mathcal{X}$ denote an instance.⁴ Fix two endpoints $\mathbf{x}^0, \mathbf{x}^1 \in \mathcal{X}$ (baseline and counterfactual). For any coalition $S \subseteq N$, define the mixed input $\mathbf{x}^S \in \mathcal{X}$ coordinatewise by

$$x_i^S := \begin{cases} x_i^1, & i \in S, \\ x_i^0, & i \notin S. \end{cases} \quad (1)$$

Define the finite-change coalition value [20, 26] by $V(S) := g(\mathbf{x}^S) - g(\mathbf{x}^0)$ for $S \subseteq N$, so $V(\emptyset) = 0$ and

$$\Delta y := V(N) = g(\mathbf{x}^1) - g(\mathbf{x}^0). \quad (2)$$

For every nonempty $u \subseteq N$, define the Möbius/Harsanyi dividend [12] by

$$\phi_u := \sum_{T \subseteq u} (-1)^{|u|-|T|} V(T). \quad (3)$$

All interaction pots in S reconstruct V (Möbius inversion [12]):

$$V(S) = \sum_{u \subseteq S} \phi_u \text{ for all } S \subseteq N, \quad \Delta y = \sum_{\emptyset \neq u \subseteq N} \phi_u. \quad (4)$$

3.2 Counterfactual analysis on local cube restriction

Fix a nonempty coalition $u \subseteq N$ with $|u| = k$, let $\Delta_i := x_i^1 - x_i^0$, and let $(e_i)_{i \in N}$ be the canonical basis of \mathbb{R}^d . Let $t = (t_i)_{i \in u} \in [0, 1]^k$, and define the cube-restricted path by

$$\mathbf{x}_u(t) := \mathbf{x}^0 + \sum_{i \in u} t_i \Delta_i e_i, \quad t \in [0, 1]^k, \quad (5)$$

⁴ If baseline/counterfactual objects are rows of a data matrix $\mathbf{X} \in \mathbb{R}^{n \times d}$, then $\mathbf{x}^0, \mathbf{x}^1$ can be read as two fixed rows (two instances), and $\mathbf{x}_u(t)$ is defined coordinatewise exactly as in (5).

and set the model $g_u(t) := g(\mathbf{x}_u(t))$. Only coordinates in u vary continuously from baseline to counterfactual *via* $t_i \in [0, 1]$. Corners $t \in \{0, 1\}^k$ correspond to full switches of selected features. Evaluations on faces (masking) are obtained by fixing some coordinates at baseline, *i.e.*, setting $t_i = 0$ for masked features. *Corners.* For any $T \subseteq u$, define $t^T \in \{0, 1\}^k$ by $(t^T)_i = 1$ if $i \in T$ and $(t^T)_i = 0$ otherwise. Then $\mathbf{x}_u(t^T) = \mathbf{x}^T$ and $g_u(t^T) = g(\mathbf{x}^T)$, for $T \subseteq u$. *Masking.* For $T \subseteq u$ and $t \in [0, 1]^k$, define the masked slider vector $t^{(T)} \in [0, 1]^k$:

$$(t^{(T)})_i := \begin{cases} t_i, & i \in T, \\ 0, & i \in u \setminus T. \end{cases}$$

Thus $g_u(t^{(T)})$ evaluates the face where only features in T may move.

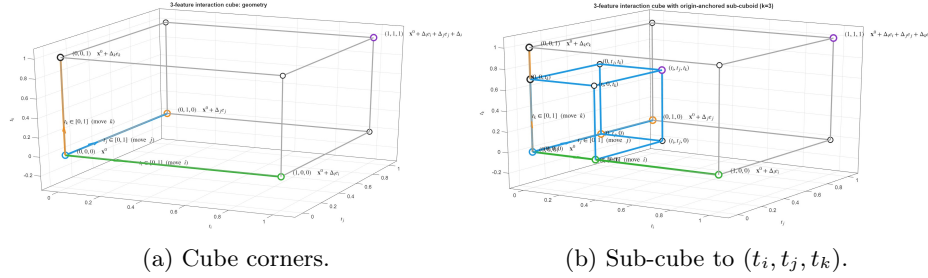


Fig. 1: Local slider cube for $u = \{i, j, k\}$ (left) and the sub-cube from $(0, 0, 0)$ to (t_i, t_j, t_k) (right), illustrating corner evaluations and the inclusion–exclusion construction.

Definition 1 (Harsanyi dividend on a local-cube). Fix $u \subseteq N$ with $|u| = k \geq 2$ and the cube-restricted model $g_u : [0, 1]^k \rightarrow \mathbb{R}$. The pure u -way residual interaction is the inclusion–exclusion surface

$$r_u(t) := \sum_{T \subseteq u} (-1)^{k-|T|} g_u(t^{(T)}), \quad t \in [0, 1]^k. \quad (6)$$

Proposition 1 (Properties). Let $u \subseteq N$ with $|u| = k \geq 2$.

- (i) If $t_i = 0$ for some $i \in u$, then $r_u(t) = 0$. (Boundary)
- (ii) At the far corner, $r_u(\mathbf{1}_k) = \phi_u$. (Efficiency)

(i) The joint presence of all k features should disappear as soon as one feature is fully “switched off” by masking. (ii) At the far corner, the Harsanyi pot is recovered when all features in u are fully moved to their counterfactual level.

3.3 Discretization of the cube on a grid & TU-micro-game

The residual interaction $r_u(t)$ describes how the interaction between features builds up inside the cube. To redistribute the interaction pot ϕ_u in a geometry-aware way, we discretize the cube and treat elementary step moves as players. Fix a resolution profile $\mathbf{m} = (m_i)_{i \in u}$ with $m_i \geq 1$ and restrict each slider to $0, \frac{1}{m_i}, \frac{2}{m_i}, \dots, 1$. A grid node is indexed by

$$p = (p_i)_{i \in u} \in \prod_{i \in u} \{0, 1, \dots, m_i\}, \quad t(p) = \left(\frac{p_i}{m_i} \right)_{i \in u} \in [0, 1]^k.$$

Definition 2 (Grid discretization). Fix $u \subseteq N$ with $|u| = k \geq 2$ and $\mathbf{m} = (m_i)_{i \in u}$ with $m_i \geq 1$. Define the sampled cube table $g_p := g_u(t(p))$. For $T \subseteq u$, define the masked index $p^{(T)}$ by keeping p_i for $i \in T$ and setting $p_i = 0$ for $i \in u \setminus T$. The discrete residual interaction table is given by:

$$r_p := \sum_{T \subseteq u} (-1)^{k-|T|} g_{p^{(T)}}. \quad (7)$$

The grid discretization is consistent, *i.e.* the table (r_p) is exactly the residual interaction surface sampled on the grid $r_p = r_u(t(p))$. In particular, $r_p = 0$ when any coordinate is still at baseline (boundary property), and $r_{\mathbf{m}} = \phi_u$ at the far corner.

Fix $i \in u$ and let e_i be the unit vector in the i -direction in index space. For any p with $p_i < m_i$, a local change on the grid is given by:

$$\Delta_p(i) := r_{p+e_i} - r_p.$$

This provides a local change in the pure interaction pot when feature i advances by one discretization step, given the current context p (*i.e.*, how far the other features have already moved).⁵ Discretization replaces each feature move $0 \rightarrow 1$ by m_i elementary steps. These steps are defined to be *micro-players* on a TU-micro-game.

Definition 3 (Micro-players and TU-micro-game). Fix $u \subseteq N$ with $|u| = k \geq 2$ and $\mathbf{m} = (m_i)_{i \in u}$ with $m_i \geq 1$. Define $N'_u := \bigcup_{i \in u} (\{i\} \times \{1, \dots, m_i\})$, so $|N'_u| = \sum_{i \in u} m_i$. For a micro-coalition $A \subseteq N'_u$, define $c_i(A) := |\{s \in \{1, \dots, m_i\} : (i, s) \in A\}| \in \{0, 1, \dots, m_i\}$. The TU-micro-game is defined as:

$$v_u : 2^{N'_u} \rightarrow \mathbb{R}, \quad \text{such that } v_u(A) := r_{p(A)} \quad \text{and } v_u(\emptyset) = 0.$$

For all moves, $v_u(N'_u) = r_{\mathbf{m}} = \phi_u$, the interaction pot is recovered. For $(i, s) \notin A$, adding the micro-player increases $c_i(A)$ by one, hence moves the state from $p(A)$ to $p(A) + e_i$ (with $p(A) := (c_i(A))_{i \in u}$). Therefore the marginal contribution of a micro-player equals the residual interaction increment:

$$v_u(A \cup \{(i, s)\}) - v_u(A) = r_{p(A)+e_i} - r_{p(A)} = \Delta_{p(A)}(i).$$

This identity links within-cube interaction geometry (the increments $\Delta_p(i)$) to cooperative-game allocation on v_u , enabling feature-level attributions by aggregating micro-player payoffs (Section 4).

⁵ When a coordinate in u is categorical, intermediate values in (5) may not be valid inputs. We therefore evaluate interior points by an endpoint-mixture that preserves all cube corners (and therefore preserves $V(\cdot)$ and the pots (ϕ_u)). For a single categorical coordinate $i \in u$, we define,

$$g_u^*(t) := (1 - t_i) g(\mathbf{x}_{u,i}^0(t)) + t_i g(\mathbf{x}_{u,i}^1(t)).$$

Thus $V(\cdot)$ and (ϕ_u) are unchanged, but the interior geometry is that of the mixture extension g_u^* rather than the raw model on invalid intermediate categorical inputs.

4 Aumann-SHAP

4.1 Interaction, local and global explainability

A value (attribution method) applied to v_u produces payoffs for micro-game players (step moves). A *feature-level* within-pot attribution is built by summing the micro-players that belong to the same feature. A value is a function φ on Γ^u , i.e. $\varphi : \Gamma^u \rightarrow \mathbb{R}^{N'_u}$, that assigns a payoff vector $\varphi(v) = (\varphi_a(v))_{a \in N'_u}$ to each TU-micro-game $v_u \in \Gamma^u$. The Shapley value [26] is the unique value satisfying Efficiency (**E**), Symmetry (**S**), Additivity (**A**), and the Null player (**N**).⁶

Theorem 1 (Micro-player Shapley value). *A value φ on Γ^u satisfies **E**, **S**, **A** and **N** if, and only if, for every micro-player $(i, s) \in N'_u$,*

$$\varphi_{(i,s)}^{\text{Sh}}(v_u) = \sum_{A \subseteq N'_u \setminus \{(i,s)\}} \frac{|A|! (|N'_u| - |A| - 1)!}{|N'_u|!} \left(v_u(A \cup \{(i,s)\}) - v_u(A) \right).$$

Interaction explainability. The term inside parenthesis is the marginal increase in interaction when one elementary step is added. The marginal moves are driven by the local increments $\Delta_p(i)$, therefore the Shapley value $\varphi_{(i,s)}^{\text{Sh}}$ is the average of all feature interactions over the sub-cube (see Supplementary materials for the proofs of theorems and propositions). For each feature $i \in u$, we define the feature-level interaction contribution by aggregation:

$$S_{i \rightarrow u}^{\text{Sh}} := \sum_{s=1}^{m_i} \varphi_{(i,s)}^{\text{Sh}}(v_u).$$

Then, $S_{i \rightarrow u}^{\text{Sh}}$ yields the contribution of feature i to the entire interaction pot ϕ_u .

Local and global explainability. Local explainability is issued from all possible within-pot shares including feature i , i.e. $S_{i \rightarrow u}^{\text{Sh}}$ (for all u), and the contribution of i alone, for one given instance:

$$S_i^{\text{Sh}} := \phi_{\{i\}} + \sum_{\substack{u \subseteq N: i \in u \\ |u| \geq 2}} S_{i \rightarrow u}^{\text{Sh}}.$$

This yields the explained variation $g(\mathbf{x}^1) - g(\mathbf{x}^0)$ for one given instance of the test data. Global explainability (for each feature i) is obtained by averaging local contributions, over the test data, in which i participates. By efficiency, the global feature explainabilities sum to the explained variation on test data.

⁶ **Efficiency (E).** For each $v_u \in \Gamma^u$, $\sum_{a \in N'_u} \varphi_a(v_u) = v_u(N'_u)$.

Symmetry (S). For each $v_u \in \Gamma^u$, for any permutation σ of N'_u , define $(\sigma v_u)(A) := v_u(\sigma^{-1}(A))$. Then, for all $a \in N'_u$, $\varphi_{\sigma(a)}(\sigma v_u) = \varphi_a(v_u)$.

Additivity (A). For each $v_u, v'_u \in \Gamma^u$, $\varphi(v_u + v'_u) = \varphi(v_u) + \varphi(v'_u)$.

Null player (N). For each $v_u \in \Gamma^u$, if a is null, i.e. $v_u(S \cup \{a\}) = v_u(S)$ for all $S \subseteq N'_u \setminus \{a\}$, then $\varphi_a(v_u) = 0$.

Proposition 2 (Equal-split Shapley [19]). *If $m_i = 1$ for every $i \in u$, then $v_u(A) = 0$ for all $A \subsetneq N'_u$ and $v_u(N'_u) = \phi_u$. Therefore,*

$$S_i^{\text{Sh}}(u) = \frac{\phi_u}{|u|}, \quad \forall i \in u.$$

The previous Proposition 2 shows that the result of [19] is a special case for one single move $m_i = 1$. This particular case is less informative: each feature i in the interaction pot $\phi(u)$ receives exactly the same contribution. Refining the grid on a continuum (large m) avoids this problem and produces an Aumann-Shapley path-based attribution method on the residual interaction surface (Theorem 2).

Theorem 2 (Aumann–SHAP). *Fix $u \subseteq N$ with $|u| = k \geq 2$ and a resolution profile $\mathbf{m} = (m_i)_{i \in u}$. Assume $r_u \in C^1([0, 1]^k)$. Then, for every $i \in u$,*

$$\lim_{\min_{j \in u} m_j \rightarrow \infty} S_{i \rightarrow u}^{\text{Sh}} = \int_0^1 \frac{\partial r_u}{\partial t_i}(\tau \mathbf{1}_k) d\tau.$$

Moreover, these limit contributions are efficient, $\sum_{i \in u} \int_0^1 \frac{\partial r_u}{\partial t_i}(\tau \mathbf{1}_k) d\tau = \phi_u$.⁷

4.2 Generalization to LES values

Micro-game-Shapley is one particular way to split a fixed interaction pot ϕ_u across its member features. Linear–Efficient–Symmetric (LES) values enable more attribution methods to be employed. Taking recourse to LES (in particular Linearity (**L**)⁸ instead of Additivity) enables the explained quantity fixed (pots remain the same), while *within-pot split* are differently evaluated (for robustness purpose).

Invoking **L**, **E**, and **S** implies (and is implied) by the LES family:

$$\varphi_{(i,s)}^{\text{LES}}(v_u) = \sum_{A \subseteq N'_u \setminus \{(i,s)\}} \frac{|A|!(n - |A| - 1)!}{n!} \left(b(|A|+1) v_u(A \cup \{(i,s)\}) - b(|A|) v_u(A) \right),$$

where $n := |N'_u|$ and $b(\cdot)$ is a scalar sequence with $b(0) = 0$ and $b(n) = 1$, see [3, 5, 6, 22, 24]. Aggregating micro-players back to a feature-level yields:

$$S_{i \rightarrow u}^{\text{LES}} := \sum_{s=1}^{m_i} \varphi_{(i,s)}^{\text{LES}}(v_u), \quad \forall i \in u.$$

By efficiency, within-pot share gives *interaction explainability* $S_{i \rightarrow u}^{\text{LES}}$. On the other hand, *local explainability* is given by $\phi_{\{i\}} + \sum_{\substack{u \subseteq N: i \in u \\ |u| \geq 2}} S_{i \rightarrow u}^{\text{LES}} = S_i^{\text{LES}}$ for one

⁷ Theorem 2 should be read as a smooth-case limit result. For non-smooth models (e.g. tree ensembles), our attribution method is still defined through finite grid evaluations of r_u , while convergence to a path-integral limit is left outside the scope of the theorem.

⁸ **Linearity (L).** For each $v_u, w_u \in \Gamma^u$ and $\alpha_1, \alpha_2 \in \mathbb{R}$, $\varphi(\alpha_1 v_u + \alpha_2 w_u) = \alpha_1 \varphi(v_u) + \alpha_2 \varphi(w_u)$.

given instance (whereas *global explainability* is obtained by averaging on test data). LES attribution methods change only *how* ϕ_u is divided, not what is being explained. As shown by [7], comparing several LES attribution methods reports explanations that are stable across rules (*e.g.*, agreement on top features), and may provide faster computation rule to be employed such as ES (see Table 1).

LES value	Choice of $b(s)$ (for $1 \leq s \leq n - 1$)	Complexity (per pot u)
Shapley value	$b(s) = 1$	$\mathcal{O}(k(m + 1)^k)$
Solidarity value	$b(s) = \frac{1}{s+1}$	$\mathcal{O}(k(m + 1)^k)$
Equal Surplus (ES)	$b(1) = n - 1, b(s) = 0 (s \geq 2)$	$\mathcal{O}(k)$

Table 1: Three LES instantiations ($n = \sum_{j \in u} m_j, k = |u|$).

5 Experiments

We first evaluate Aumann-SHAP and its complexity over an exact grid-state computation. Second, we compare LES explainability (interaction, local and global) on the German Credit dataset [33], and finally on MNIST data [18] to assess which pixels may cause false positives during the transition $1 \rightarrow 7$.⁹

5.1 Simulations: Exact computation and complexity

Direct computation of Shapley/LES on v_u over N'_u (with $n = \sum_{j \in u} m_j$ micro-players) requires summing over 2^n micro-coalitions, *i.e.* $\mathcal{O}(n 2^n)$ operations per interaction pot. The key structure of our induced TU-micro-game is $v_u(A) = r_{p(A)}$, therefore the game v_u depends only on its *grid state* $p(A)$. We can therefore group terms by states by defining $\Delta_p(i) := b(|p| + 1)r_{p+e_i} - b(|p|)r_p$, if $p_i < m_i$, and 0 otherwise.

Proposition 3 (LES closed form). *Fix $u \subseteq N$ with $|u| \geq 2$ and $\mathbf{m} = (m_j)_{j \in u}$, and let $n = \sum_{j \in u} m_j$. Then, for every $i \in u$,*

$$S_{i \rightarrow u}^{\text{LES}} = \sum_{\substack{p \in \mathcal{G}(u) \\ p_i < m_i}} \frac{|p|!(n - |p| - 1)!}{n!} \left(\prod_{j \in u} \binom{m_j}{p_j} \right) (m_i - p_i) \Delta_p(i). \quad (8)$$

Complexity. In the uniform-resolution regime $m_j \equiv m$ (so $n = km$), full enumeration costs $\mathcal{O}(km 2^{km})$. Eq. (8) loops over $(m + 1)^k$ states and k directions, yielding $\mathcal{O}(k(m + 1)^k)$, polynomial in m for fixed k (and exponential only in k). Equal Surplus is $\mathcal{O}(k)$ once the needed corner quantities are computed [7]. Empirically, the reduction is decisive as shown in Figure 2. At fixed $k = 3$, increasing m quickly makes full enumeration infeasible, while the grid-state method remains fast. At fixed $m = 4$, grid-state runtimes grow as $(m + 1)^k$ while full enumeration grows as 2^{km} .

⁹ See our [repository](#).

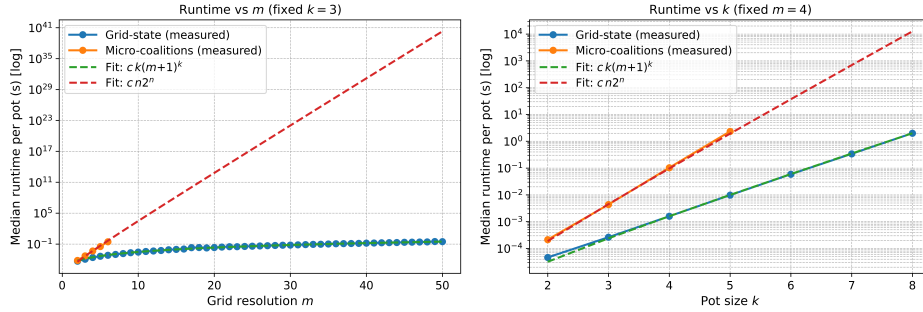


Fig. 2: Solid curves with markers provide runtimes: grid-state computation (blue) and, when feasible, full micro-coalition enumeration (orange). Dashed curves are fitted scaling laws: $\sim c k(m+1)^k$ for grid-state (green) and $\sim c n 2^n$ with $n=km$ for full enumeration (red).

Convergence. The Riemann sum converges to the Aumann–Shapley integral at rate $\mathcal{O}(1/n)$, which can also depend on model regularity along the interpolation path (see Supplementary materials). For smooth models (*e.g.* GLM see Table 2), residual interaction increments vary gradually across states and moderate m is sufficient. For threshold predictors (tree ensembles, boosted trees), attributions may change when refinement resolves new split thresholds, larger m improves stability while remaining tractable *via* the grid-state formula.¹⁰

Model class	Typical m (our simulations)	Default recommendation
GLM regressions (smooth, linear)	$m \approx 4\text{--}6$	start at $m = 5$
MLP (smooth, differentiable)	$m \approx 6\text{--}10$	start at $m = 8$
XGBoost / GBDT (thresholded, piecewise)	$m \approx 8\text{--}15$	start at $m = 10$

Table 2: Typical grid resolutions required for stable attributions in our experiments.

5.2 German credit

The German Credit dataset [15] contains applicant-level information describing loan requests, financial situation, and basic demographic characteristics, with labels *creditworthy* vs. *not creditworthy*. We use the standard pre-processed benchmark (27 attributes, 1,000 applicants) popularized in [33] and adopted in [19]. Our goal is to explain *counterfactual transitions* from a baseline \mathbf{x}^0 (not creditworthy) to a successful counterfactual \mathbf{x}^1 (creditworthy), in order to outline *interactions* responsibility among changed features.

Three independent classifiers are trained (logistic regression, MLP, XGBoost) and combine their predicted probabilities into a conservative score,

$$p_{\min 3}(\mathbf{x}) = \min\{p_{\text{logistic}}(\mathbf{x}), p_{\text{mlp}}(\mathbf{x}), p_{\text{xgboost}}(\mathbf{x})\}.$$

¹⁰ We apply a conservative saturation rule: increase m until the maximum absolute change in any feature share between successive m values is below a tolerance ε (*e.g.*, 0.1 percentage points) for a few consecutive refinements (*e.g.*, three), and report the resulting attributions.

We focus on a representative individual (idx 242) with low baseline confidence and generate three successful counterfactuals using complementary procedures: (i) a DiCE-style randomized search, (ii) Growing Spheres, and (iii) a genetic algorithm. For all methods the same strict success condition is imposed, $p_{\min 3}(\mathbf{x}^1) \geq 0.8$, so differences across explanations are *not* about success vs. failure, but about how the gain $\Delta V = p_{\min 3}(\mathbf{x}^1) - p_{\min 3}(\mathbf{x}^0)$ is attributed.

Local explainability [Tab. 3]. For each counterfactual scenario, we explain the same improvement ΔV using three attribution methods: (i) the counterfactual equal-split Shapley baseline ϕ^{eq} [19], (ii) Micro-game Shapley S^{micro} (our method with uniform grid $m = 5$), and (iii) Equal Surplus (ES) as an LES baseline [7]. All three satisfy efficiency (feature local explanations sum to ΔV). The key question is therefore not what is explained, but *where responsibility is placed* among the changed features. The Growing Spheres scenario [Tab. 3] is $X_8 : 0 \rightarrow 1$, $X_{13} : 1 \rightarrow 0$, $X_{14} : 0 \rightarrow 1$ and $X_{25} : 0 \rightarrow 1$. The dominant contributor is X_8 (X_{22} and X_8 in DiCE and Genetic scenarios respectively, see Table 2 in Supplementary materials). Beyond the top driver, the ranking of X_{13} and X_{14} differs: equal-split Shapley assigns more to X_{13} than X_{14} , whereas S^{micro} and ES assign more to X_{14} than X_{13} . Importantly, these two discrepancies have different interpretations. The gap between S^{micro} and ϕ^{eq} is explained by *interaction geometry*: equal-split Shapley enforces a symmetric division within each interaction pot, while micro-game Shapley redistributes them according to how interaction gains accumulate inside the local cube.¹¹

Growing Spheres counterfactual				$(\Delta V = 0.6569)$	
Feature	ϕ^{eq}	S^{micro}	ES	$S^{\text{micro}} - \phi^{\text{eq}}$	$S^{\text{micro}} - ES$
X_8 (<i>Checking account</i>)	0.3331	0.4389	0.3013	+16.11%	+20.95%
X_{14} (<i>Loans Elsewhere</i>)	0.1295	0.1130	0.1576	-2.50%	-6.79%
X_{13} (<i>Credit history</i>)	0.1772	0.0934	0.1313	-12.77%	-5.77%
X_{25} (<i>Housing</i>)	0.0171	0.0115	0.0666	-0.85%	-8.39%

Table 3: Feature-level totals under equal splitting (ϕ^{eq}), TU-micro-game Shapley (S^{micro}), and Equal Surplus in Δ -units (ES). Columns 4 and 5: % computed on ΔV .

Interaction explainability [Tab. 4]. The main contribution of Aumann-SHAP is to explain local explainability, accounting for the interaction between features. The micro-game Shapley shifts a substantial share of the gain toward X_8 and away from X_{13} relative to the equal-split baseline. Indeed, X_{13} (*Credit history*) tends to decrease the transition to creditworthiness (0.0176) while X_8 (*Checking account*) improves it a lot (0.1143). On the contrary, equal-split Shapley is silent about interaction effects since feature contributions are balanced.

¹¹ In our experiments, ES is used only as a feature-total baseline, not as a canonical within-pot decomposition.

Pot T	Feat.	ϕ^{eq}	S^{micro}	$\phi^{\text{eq}} - S^{\text{micro}}$
$X_8 + X_{13}$	X_{13}	0.0659	0.0176	-0.0484
$X_8 + X_{13}$	X_8	0.0659	0.1143	0.0484
$X_8 + X_{14}$	X_{14}	-0.0004	-0.0366	-0.0362
$X_8 + X_{14}$	X_8	-0.0004	0.0359	0.0362

Table 4: **Growing Spheres: within-pot reallocations (TU-micro-game vs. equal split).**

Global explainability and convergence. At the dataset level (see Table 7 in Supplementary materials), we aggregate over low-score baselines ($n = 144$) and generate successful counterfactuals under the same target constraint $p_{\text{xgboost}}(\mathbf{x}^1) \geq 0.80$ (with $p_{\text{xgboost}}(\mathbf{x}^0) < 0.30$ and $\bar{k} = 2.51$ changed features). The global ranking is clear, X_2 (*Loan amount*) and X_1 (*Loan duration*) dominate the average improvement. Importantly, the three attribution methods remain very close on average, indicating robustness among attribution methods.

5.3 MNIST

MNIST data [18] are used to visualize which pixels (and which pixel interactions) drive a counterfactual transition such as $1 \rightarrow 7$ (70,000 grayscale digits split into 60,000 train and 10,000 test samples). A ResNet-18 [13] architecture is trained and the resulting model attains a test accuracy of 0.9972. To construct a counterfactual transition, we select a baseline image \mathbf{x}^0 of class 1 and a target image \mathbf{x}^1 of class 7, and we restrict the feature set to 109 pixels that actually differ between the two endpoints, *i.e.* those satisfying $|x_{\text{row,col}}^1 - x_{\text{row,col}}^0| > 0.05$.

To explain $\Delta := g(\mathbf{x}_{\text{end}}) - g(\mathbf{x}^0)$, we compare the counterfactual equal-split Shapley (baseline [19]) and our micro-player Shapley attribution method. In both cases, Shapley values are estimated by Monte-Carlo permutation sampling (to avoid enumerating $2^{|N|}$ subsets or $2^{|N'|}$ micro-coalitions). Pixel-level attribution maps are reported, such that totals match Δ by efficiency [26]. Figure 3 first answers the counterfactual question “what changes make the classifier see a 7?”: the dominant positive attributions (blue) concentrate on the horizontal top stroke and the upper-right hook, *i.e.* the pixels that visually transform a thin “1” into a “7”. Negative contributions (red) appear on pixels that either preserve the “1”-like vertical structure or add mass in regions that are inconsistent with a typical “7”, thus, contributing to increase false positives.

Interaction explainability [Fig. 3]. The top-25 pixels largely overlap, showing broad agreement of the two attribution methods. The redistribution map reveals a localized reallocation of attribution mass, as micro-game Shapley (for $m = 10$) amplifies a small subset of pixels and down-weights others (highlighted in the overlay, Figure 3 at the bottom), reflecting interaction-aware responsibility along the counterfactual path rather than equal splitting (baseline Shapley). Thus, the difference D between methods is not *whether* the counterfactual succeeds (both explain the same Δ), but *where* responsibility is placed during transition.

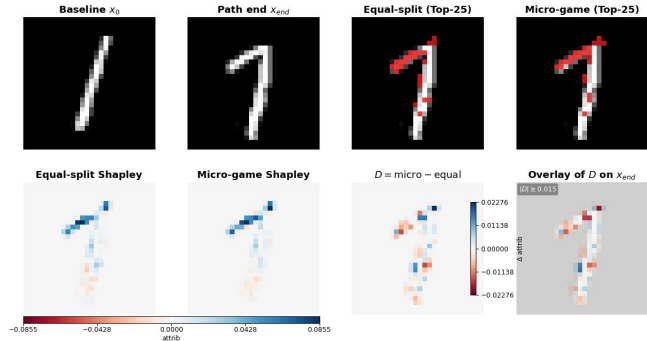


Fig. 3: MNIST 1 \rightarrow 7 counterfactual: attribution maps and redistribution. Top row: baseline x^0 , endpoint x^1 (only the k changed pixels are moved), and TOP-25 masks for equal-split and TU-micro-game Shapley (red). Bottom row: signed heatmaps, redistribution $D = \text{micro} - \text{equal}$, and an overlay of the largest re-allocations on x^1 .

Global explainability [Fig. 4]. Explanations are aggregated across many 1 \rightarrow 7 transitions and answer the question: *which pixels are reliably responsible for preventing the classifier from producing a false positive “1” instead of a true positive “7”?* Each attribution method concentrates on the characteristic “7” top bar and the upper hook region, indicating that, over the test distribution, these strokes are the most consistent drivers of the accuracy score. Concentration curves (see Figure 2 in Supplementary material) quantify *how sharply* importance is localized: micro-game and equal-split Shapley concentrate a large fraction of the mean attribution mass into a small set of pixels, while Equal Surplus spreads mass more diffusely across the digit, producing a slower accumulation.

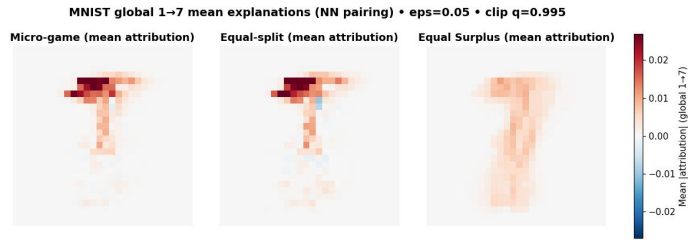


Fig. 4: Global MNIST 1 \rightarrow 7 mean explanations (nearest-neighbor pairing). We sample 200 test-set baselines x^0 of digit 1 and pair each with its nearest neighbor x^1 among test-set 7’s (Euclidean distance), then compute local attributions on the changed-pixel set $\{(r, c) : |x_{rc}^1 - x_{rc}^0| > \varepsilon\}$ with $\varepsilon = 0.05$ and average the resulting maps over pairs.

Counterfactual patch test [Fig. 5]. Starting from the baseline digit class “1”, we rank the changed pixels using each attribution method and then generate a sequence of partial counterfactuals by patching only the top- K ranked pixels from “1” toward their endpoint values in “7”. For each budget K the classifier accuracy (P_7) is computed, yielding a budget curve. An attribution method is

more accurate if it reaches a target confidence with fewer edits (smaller $K@0.5$ and $K@0.9$) and if it increases P_7 rapidly across the whole budget range.

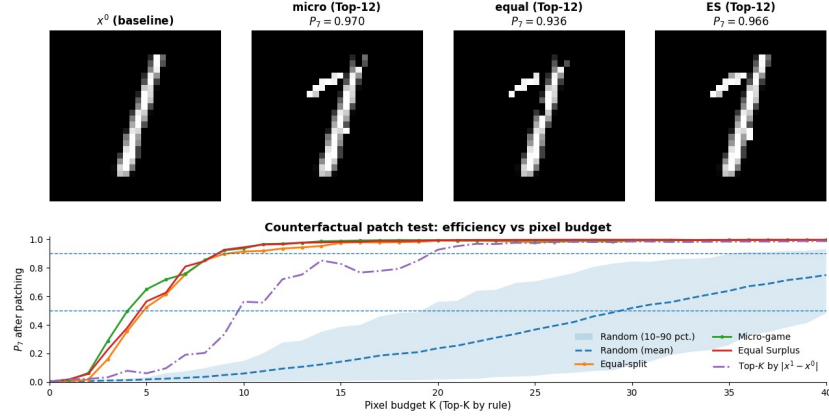


Fig. 5: Counterfactual patch test on MNIST ($1 \rightarrow 7$): P_7 after patching the top- K pixels selected by each rule (Micro-game Shapley, Equal-split Shapley, Equal surplus, and $|x^1 - x^0|$), compared to a random baseline (mean with 10–90% band). Top row shows x^0 and the patched images at $K = 12$.

Across budgets, the micro-game Shapley (the green curve) ordering rises fastest compared with the equal-split Shapley (the red curve) and ES, indicating a higher accuracy improvement with fewer patched pixels. Since all methods apply the *same* endpoint replacements (only the ranking differs), this gap isolates what is learned from the attribution rule itself. Micro-game Shapley identifies pixel changes that are most effective when applied early along the $1 \rightarrow 7$ transition.

6 Conclusion

Aumann–SHAP is a geometric attribution method for counterfactual transitions that (i) isolates pure interaction residuals on the local baseline–counterfactual cube and (ii) redistributes interaction “pots” *via* an induced TU-micro-game whose players are elementary grid-step moves. It delivers efficient local and global attributions under Shapley and LES values, admits an exact grid-state closed form with tractable complexity for fixed interaction order, and converges under grid refinement to the diagonal Aumann–Shapley / Integrated Gradients limit. Empirically, simulations confirm the scaling advantages of the grid-state approach over full micro-coalition enumeration, while the German Credit and MNIST studies show stable, meaningful attributions: key drivers are robust across allocation rules, and micro-game redistributions expose interaction-driven responsibility shifts aligned with actionable counterfactual edits.

Disclosure of Interests. The authors have no competing interests to declare.

Supplementary Material

S1 Proofs

Proof of Proposition 1 (Properties)

Statement. Fix a coalition $u \subseteq N$ with $|u| = k \geq 2$, and let $g_u : [0, 1]^k \rightarrow \mathbb{R}$ be the cube-restricted model. For $t \in [0, 1]^k$, define the masked vector $t^{(T)}$ by $(t^{(T)})_i = t_i$ if $i \in T$ and $(t^{(T)})_i = 0$ if $i \in u \setminus T$, and define the pure u -way residual

$$r_u(t) := \sum_{T \subseteq u} (-1)^{k-|T|} g_u(t^{(T)}).$$

Then:

- (i) If $t_{i_0} = 0$ for some $i_0 \in u$, then $r_u(t) = 0$ (*Boundary*).
- (ii) At the far corner, $r_u(\mathbf{1}_k) = \phi_u$ (*Efficiency*).

Proof.

(i) **Boundary vanishing.** Assume $t_{i_0} = 0$ for some $i_0 \in u$. Define the involution $\psi : \mathcal{P}(u) \rightarrow \mathcal{P}(u)$ by

$$\psi(T) := \begin{cases} T \setminus \{i_0\}, & i_0 \in T, \\ T \cup \{i_0\}, & i_0 \notin T. \end{cases}$$

Then $|\psi(T)| = |T| \pm 1$, hence $(-1)^{k-|\psi(T)|} = -(-1)^{k-|T|}$. Moreover, since $t_{i_0} = 0$, the masked vectors coincide:

$$t^{(\psi(T))} = t^{(T)},$$

because whether $i_0 \in T$ or not, the i_0 -coordinate of the masked vector equals 0. Therefore the terms indexed by T and $\psi(T)$ cancel pairwise in the sum defining $r_u(t)$, and thus $r_u(t) = 0$.

(ii) **Far-corner equals the pot.** Take $t = \mathbf{1}_k$. For each $T \subseteq u$, the masked vector $\mathbf{1}_k^{(T)}$ is the 0–1 indicator of T (ones on T and zeros on $u \setminus T$), hence $\mathbf{x}_u(\mathbf{1}_k^{(T)}) = \mathbf{x}^T$ and so $g_u(\mathbf{1}_k^{(T)}) = g(\mathbf{x}^T)$. Therefore

$$r_u(\mathbf{1}_k) = \sum_{T \subseteq u} (-1)^{k-|T|} g(\mathbf{x}^T).$$

Using $g(\mathbf{x}^T) = V(T) + g(\mathbf{x}^0)$ (so $V(T) = g(\mathbf{x}^T) - g(\mathbf{x}^0)$) yields

$$r_u(\mathbf{1}_k) = \sum_{T \subseteq u} (-1)^{k-|T|} V(T) + g(\mathbf{x}^0) \sum_{T \subseteq u} (-1)^{k-|T|} \quad (\text{S1.1})$$

$$= \phi_u + g(\mathbf{x}^0) (1 - 1)^k = \phi_u, \quad (\text{S1.2})$$

since $\phi_u = \sum_{T \subseteq u} (-1)^{k-|T|} V(T)$ and $\sum_{T \subseteq u} (-1)^{k-|T|} = (1 - 1)^k = 0$. \square

Proof of Theorem 1 (Micro-player Shapley value)

Statement. A value φ on Γ^u satisfies **E**, **S**, **A** and **N** if, and only if, for every micro-player $(i, s) \in N'_u$,

$$\varphi_{(i,s)}^{\text{Sh}}(v_u) = \sum_{A \subseteq N'_u \setminus \{(i,s)\}} \frac{|A|! (|N'_u| - |A| - 1)!}{|N'_u|!} \left(v_u(A \cup \{(i,s)\}) - v_u(A) \right).$$

Proof.

The induced map $v_u : 2^{N'_u} \rightarrow \mathbb{R}$ is an ordinary TU-game on the finite player set N'_u . Therefore, the classical Shapley characterization theorem applies directly: the unique value on games over N'_u satisfying **E**, **S**, **A** and **N** is the Shapley value. Hence, for every micro-player $(i, s) \in N'_u$,

$$\varphi_{(i,s)}(v_u) = \varphi_{(i,s)}^{\text{Sh}}(v_u),$$

with

$$\varphi_{(i,s)}^{\text{Sh}}(v_u) = \sum_{A \subseteq N'_u \setminus \{(i,s)\}} \frac{|A|! (|N'_u| - |A| - 1)!}{|N'_u|!} \left(v_u(A \cup \{(i,s)\}) - v_u(A) \right).$$

Conversely, the displayed formula is precisely the Shapley value on N'_u , and therefore satisfies **E**, **S**, **A** and **N**. \square

Feature-level within-pot shares are then obtained by aggregation:

$$S_{i \rightarrow u}^{\text{Sh}} := \sum_{s=1}^{m_i} \varphi_{(i,s)}^{\text{Sh}}(v_u), \quad i \in u.$$

Proof of Proposition 2 (Equal-split Shapley)

Statement. If $m_i = 1$ for every $i \in u$, then $v_u(A) = 0$ for all $A \subsetneq N'_u$ and $v_u(N'_u) = \phi_u$. Therefore, as in [19],

$$S_i^{\text{Sh}}(u) = \frac{\phi_u}{|u|}, \quad \forall i \in u.$$

Proof. Assume $m_i = 1$ for all $i \in u$. Then

$$N'_u = \bigcup_{i \in u} (\{i\} \times \{1\}), \quad |N'_u| = |u|,$$

and for any micro-coalition $A \subseteq N'_u$ we have $c_i(A) \in \{0, 1\}$ and hence

$$p(A) = (c_i(A))_{i \in u} \in \{0, 1\}^k, \quad v_u(A) = r_{p(A)}.$$

Step 1: identify r_p with $r_u(t(p))$ on the $\{0, 1\}^k$ grid. For $p \in \{0, 1\}^k$, recall $t(p) = (p_i)_{i \in u}$ since $m_i = 1$. By definition, $g_p = g_u(t(p))$ and

$$r_p = \sum_{T \subseteq u} (-1)^{k-|T|} g_{p^{(T)}}.$$

But when $p \in \{0, 1\}^k$, the masked index $p^{(T)}$ corresponds exactly to the masked slider vector $t(p)^{(T)}$ (keep coordinates in T and set the others to 0). Hence

$$r_p = \sum_{T \subseteq u} (-1)^{k-|T|} g_u(t(p)^{(T)}) = r_u(t(p)).$$

So for every $A \subseteq N'_u$,

$$v_u(A) = r_{p(A)} = r_u(t(p(A))). \quad (\text{S1.3})$$

Step 2: proper coalitions have zero value. If $A \subsetneq N'_u$, then there exists $i_0 \in u$ with $(i_0, 1) \notin A$, so $c_{i_0}(A) = 0$ and thus $t(p(A))_{i_0} = 0$. By Proposition 1 (i) (Boundary), this implies $r_u(t(p(A))) = 0$. Using (S1.3), we obtain $v_u(A) = 0$.

Step 3: the grand coalition equals the pot. For $A = N'_u$, we have $c_i(A) = 1$ for all $i \in u$, hence $t(p(A)) = \mathbf{1}_k$. By Proposition 1, (ii) (Efficiency),

$$v_u(N'_u) = r_{p(N'_u)} = r_u(\mathbf{1}_k) = \phi_u.$$

Step 4: Shapley splits a unanimity game equally. Steps 2–3 show that v_u is the unanimity game on the player set N'_u : it is 0 on every proper coalition and equals ϕ_u on N'_u . The Shapley value therefore assigns each micro-player the payoff $\phi_u/|N'_u| = \phi_u/|u|$. Since each feature $i \in u$ has exactly one micro-player $(i, 1)$, the aggregated feature share is

$$S_i^{\text{Sh}}(u) = \varphi_{(i,1)}^{\text{Sh}}(v_u) = \frac{\phi_u}{|u|}, \quad i \in u,$$

which proves the proposition. \square

Proof of Theorem 2 (Aumann–Shapley)

Statement. Fix $u \subseteq N$ with $|u| = k \geq 2$ and a resolution profile $\mathbf{m} = (m_i)_{i \in u}$. Assume $r_u \in C^1([0, 1]^k)$. Then, for every $i \in u$,

$$\lim_{\min_{j \in u} m_j \rightarrow \infty} S_{i \rightarrow u}^{\text{Sh}} = \int_0^1 \frac{\partial r_u}{\partial t_i}(\tau \mathbf{1}_k) d\tau,$$

and moreover these limit shares are efficient:

$$\sum_{i \in u} \int_0^1 \frac{\partial r_u}{\partial t_i}(\tau \mathbf{1}_k) d\tau = \phi_u.$$

Proof. Fix $i \in u$ and write

$$m_{\min} := \min_{j \in u} m_j, \quad N'_u := \bigcup_{j \in u} (\{j\} \times \{1, \dots, m_j\}), \quad n := |N'_u| = \sum_{j \in u} m_j.$$

Let $\Pi = (\Pi_1, \dots, \Pi_n)$ be a uniform random permutation of N'_u and define

$$A_t := \{\Pi_1, \dots, \Pi_t\} \subseteq N'_u, \quad t = 0, 1, \dots, n,$$

with $A_0 = \emptyset$. Recall that $v_u(A) = r_{p(A)}$ where $p(A) = (c_j(A))_{j \in u}$ and $c_j(A)$ counts how many replicas of feature j belong to A .

Step 1: Random-order representation of the aggregated Shapley share. For any TU game v on player set N'_u and any player $a \in N'_u$, the Shapley value admits the random-permutation form

$$\varphi_a^{\text{Sh}}(v) = \mathbb{E} \left[v(A_{\text{pos}(a)-1} \cup \{a\}) - v(A_{\text{pos}(a)-1}) \right],$$

where $\text{pos}(a)$ is the position of a in Π . Summing over the m_i replicas of feature i and rewriting by time index gives

$$S_{i \rightarrow u}^{\text{Sh}} = \mathbb{E} \left[\sum_{t=0}^{n-1} \mathbf{1}_{\{\Pi_{t+1} \in \{i\} \times \{1, \dots, m_i\}\}} \left(v_u(A_t \cup \{\Pi_{t+1}\}) - v_u(A_t) \right) \right]. \quad (\text{S1.4})$$

Step 2: Express marginals as one-step residual differences. On the event $\{\Pi_{t+1} = (i, s)\}$, adding one replica of i increases $c_i(A_t)$ by one and leaves all other counts unchanged, so $p(A_t \cup \{(i, s)\}) = p(A_t) + e_i$. Hence,

$$v_u(A_t \cup \{(i, s)\}) - v_u(A_t) = r_{p(A_t) + e_i} - r_{p(A_t)}.$$

By the grid construction, r_p is the residual surface sampled at $t(p) := (p_j/m_j)_{j \in u}$, i.e. $r_p = r_u(t(p))$ (grid consistency), and $t(p + e_i) = t(p) + \frac{1}{m_i} e_i$. Therefore (S1.4) becomes

$$S_{i \rightarrow u}^{\text{Sh}} = \mathbb{E} \left[\sum_{t=0}^{n-1} \mathbf{1}_{\{\Pi_{t+1} \in \{i\} \times \{1, \dots, m_i\}\}} \left(r_u(t(p(A_t)) + \frac{1}{m_i} e_i) - r_u(t(p(A_t))) \right) \right]. \quad (\text{S1.5})$$

Step 3: Mean-value expansion. Since $r_u \in C^1([0, 1]^k)$, for each t such that $\Pi_{t+1} \in \{i\} \times \{1, \dots, m_i\}$, the 1D mean-value theorem along direction e_i yields a (random) $\theta_t \in (0, 1)$ such that

$$r_u(t(p(A_t)) + \frac{1}{m_i} e_i) - r_u(t(p(A_t))) = \frac{1}{m_i} \frac{\partial r_u}{\partial t_i} \left(t(p(A_t)) + \frac{\theta_t}{m_i} e_i \right).$$

Plugging into (S1.5) gives

$$S_{i \rightarrow u}^{\text{Sh}} = \frac{1}{m_i} \mathbb{E} \left[\sum_{t=0}^{n-1} \mathbf{1}_{\{\Pi_{t+1} \in \{i\} \times \{1, \dots, m_i\}\}} \frac{\partial r_u}{\partial t_i} \left(t(p(A_t)) + \frac{\theta_t}{m_i} e_i \right) \right]. \quad (\text{S1.6})$$

Step 4: The random grid state concentrates near the diagonal. For each $j \in u$, define $C_j(t) := c_j(A_t)$, so that

$$t(p(A_t)) = \left(\frac{C_j(t)}{m_j} \right)_{j \in u}.$$

Let $U_{j,1}, \dots, U_{j,m_j} \in \{1, \dots, n\}$ be the random positions in Π of the m_j replicas of feature j . Then

$$C_j(t) = \sum_{s=1}^{m_j} \mathbf{1}\{U_{j,s} \leq t\}, \quad \frac{C_j(t)}{m_j} = \frac{1}{m_j} \sum_{s=1}^{m_j} \mathbf{1}\left\{ \frac{U_{j,s}}{n} \leq \frac{t}{n} \right\}.$$

Using a DKW-type bound for sampling without replacement (or equivalently Hoeffding-type concentration for the hypergeometric process), for every $\varepsilon > 0$,

$$\mathbb{P} \left(\max_{0 \leq t \leq n} \left| \frac{C_j(t)}{m_j} - \frac{t}{n} \right| \geq \varepsilon \right) \leq 2e^{-2m_j\varepsilon^2}.$$

A union bound over $j \in u$ yields

$$\mathbb{P} \left(\max_{j \in u} \max_{0 \leq t \leq n} \left| \frac{C_j(t)}{m_j} - \frac{t}{n} \right| \geq \varepsilon \right) \leq 2k e^{-2m_{\min}\varepsilon^2} \xrightarrow{m_{\min} \rightarrow \infty} 0. \quad (\text{S1.7})$$

Step 5: Replace evaluation points by the diagonal. Let $B := \sup_{x \in [0,1]^k} |\partial_i r_u(x)| < \infty$ and define the modulus of continuity

$$\omega(\delta) := \sup \left\{ |\partial_i r_u(x) - \partial_i r_u(y)| : \|x - y\|_\infty \leq \delta \right\}, \quad \omega(\delta) \downarrow 0 \text{ as } \delta \downarrow 0.$$

On the event

$$E_{\mathbf{m}}(\varepsilon) := \left\{ \max_{0 \leq t \leq n} \left\| t(p(A_t)) - \frac{t}{n} \mathbf{1}_k \right\|_\infty \leq \varepsilon \right\},$$

we have for all t ,

$$\left\| \left(t(p(A_t)) + \frac{\theta_t}{m_i} e_i \right) - \frac{t}{n} \mathbf{1}_k \right\|_\infty \leq \varepsilon + \frac{1}{m_i} \leq \varepsilon + \frac{1}{m_{\min}},$$

hence

$$\left| \partial_i r_u \left(t(p(A_t)) + \frac{\theta_t}{m_i} e_i \right) - \partial_i r_u \left(\frac{t}{n} \mathbf{1}_k \right) \right| \leq \omega \left(\varepsilon + \frac{1}{m_{\min}} \right).$$

Also, $\sum_{t=0}^{n-1} \mathbf{1}\{\Pi_{t+1} \in \{i\} \times \{1, \dots, m_i\}\} = m_i$ deterministically. Therefore, from (S1.6) we obtain

$$S_{i \rightarrow u}^{\text{Sh}} = \frac{1}{m_i} \mathbb{E} \left[\sum_{t=0}^{n-1} \mathbf{1}\{\Pi_{t+1} \in \{i\} \times \{1, \dots, m_i\}\} \partial_i r_u \left(\frac{t}{n} \mathbf{1}_k \right) \right] + o(1),$$

where $o(1) \rightarrow 0$ as $m_{\min} \rightarrow \infty$ (use (S1.7) and then let $\varepsilon \downarrow 0$).

Step 6: Compute the expectation and pass to a Riemann limit. For each t , by symmetry of a uniform permutation,

$$\mathbb{P}(\Pi_{t+1} \in \{i\} \times \{1, \dots, m_i\}) = \frac{m_i}{n}.$$

Hence,

$$\mathbb{E} \left[\mathbf{1}\{\Pi_{t+1} \in \{i\} \times \{1, \dots, m_i\}\} \partial_i r_u \left(\frac{t}{n} \mathbf{1}_k \right) \right] = \frac{m_i}{n} \partial_i r_u \left(\frac{t}{n} \mathbf{1}_k \right),$$

and therefore

$$S_{i \rightarrow u}^{\text{Sh}} = \frac{1}{n} \sum_{t=0}^{n-1} \partial_i r_u \left(\frac{t}{n} \mathbf{1}_k \right) + o(1).$$

Since $\tau \mapsto \partial_i r_u(\tau \mathbf{1}_k)$ is continuous on $[0, 1]$ and $n = \sum_{j \in u} m_j \rightarrow \infty$ as $m_{\min} \rightarrow \infty$, these Riemann sums converge:

$$\frac{1}{n} \sum_{t=0}^{n-1} \partial_i r_u \left(\frac{t}{n} \mathbf{1}_k \right) \longrightarrow \int_0^1 \partial_i r_u(\tau \mathbf{1}_k) d\tau.$$

Which is the desired result.

Efficiency of the limit. By the chain rule, for $\tau \in [0, 1]$,

$$\frac{d}{d\tau} r_u(\tau \mathbf{1}_k) = \sum_{i \in u} \frac{\partial r_u}{\partial t_i}(\tau \mathbf{1}_k).$$

Integrating from 0 to 1 gives

$$\sum_{i \in u} \int_0^1 \frac{\partial r_u}{\partial t_i}(\tau \mathbf{1}_k) d\tau = r_u(\mathbf{1}_k) - r_u(\mathbf{0}).$$

By Proposition 1, $r_u(\mathbf{1}_k) = \phi_u$ and $r_u(\mathbf{0}) = 0$, hence the sum equals ϕ_u , which proves efficiency. \square

Proof of Proposition 3 (LES closed form)

Statement. Fix $u \subseteq N$ with $|u| \geq 2$ and $\mathbf{m} = (m_j)_{j \in u}$, and let $n = \sum_{j \in u} m_j$. Then, for every $i \in u$,

$$S_{i \rightarrow u}^{\text{LES}} = \sum_{\substack{p \in \mathcal{G}(u) \\ p_i < m_i}} \frac{|p|! (n - |p| - 1)!}{n!} \left(\prod_{j \in u} \binom{m_j}{p_j} \right) (m_i - p_i) \Delta_p(i),$$

where $|p| := \sum_{j \in u} p_j$ and (as defined in the text)

$$\Delta_p(i) := b(|p| + 1) r_{p+e_i} - b(|p|) r_p \quad \text{for } p_i < m_i.$$

Proof. Let

$$N'_u := \bigcup_{j \in u} (\{j\} \times \{1, \dots, m_j\}), \quad n := |N'_u| = \sum_{j \in u} m_j,$$

and recall the induced TU-micro-game $v_u(A) = r_{p(A)}$, where the grid-state map is

$$p(A) = (c_j(A))_{j \in u}, \quad c_j(A) := |\{s : (j, s) \in A\}| \in \{0, \dots, m_j\}.$$

In particular, for any $A \subseteq N'_u$, we have $|A| = \sum_{j \in u} c_j(A) = |p(A)|$.

Fix a micro-player $(i, s) \in N'_u$. By the LES formula given in the paper,

$$\varphi_{(i,s)}^{\text{LES}}(v_u) = \sum_{A \subseteq N'_u \setminus \{(i,s)\}} \frac{|A|! (n - |A| - 1)!}{n!} \left(b(|A|+1) v_u(A \cup \{(i,s)\}) - b(|A|) v_u(A) \right).$$

For each such A , adding (i, s) increases $c_i(A)$ by 1 and leaves all other counts unchanged, hence $p(A \cup \{(i, s)\}) = p(A) + e_i$. Therefore,

$$v_u(A) = r_{p(A)}, \quad v_u(A \cup \{(i, s)\}) = r_{p(A)+e_i},$$

and the bracket becomes

$$b(|p(A)| + 1) r_{p(A)+e_i} - b(|p(A)|) r_{p(A)} = \Delta_{p(A)}(i).$$

Thus the summand depends on A only through its grid state $p(A)$. We can group coalitions by p :

$$\varphi_{(i,s)}^{\text{LES}}(v_u) = \sum_{\substack{p \in \mathcal{G}(u) \\ p_i \leq m_i - 1}} \frac{|p|! (n - |p| - 1)!}{n!} \#\{A \subseteq N'_u \setminus \{(i, s)\} : p(A) = p\} \Delta_p(i).$$

For a fixed p with $p_i \leq m_i - 1$, the number of coalitions $A \subseteq N'_u \setminus \{(i, s)\}$ satisfying $p(A) = p$ is

$$\binom{m_i - 1}{p_i} \prod_{j \in u \setminus \{i\}} \binom{m_j}{p_j},$$

since we must choose p_i replicas of feature i from the remaining $m_i - 1$ (excluding (i, s)), and independently choose p_j replicas of each other feature j from its m_j replicas.

Now aggregate replicas back to the feature level:

$$S_{i \rightarrow u}^{\text{LES}} := \sum_{s=1}^{m_i} \varphi_{(i,s)}^{\text{LES}}(v_u).$$

Summing the above expression over $s = 1, \dots, m_i$ multiplies the counting term by m_i , giving

$$S_{i \rightarrow u}^{\text{LES}} = \sum_{\substack{p \in \mathcal{G}(u) \\ p_i \leq m_i - 1}} \frac{|p|! (n - |p| - 1)!}{n!} \left(m_i \binom{m_i - 1}{p_i} \prod_{j \neq i} \binom{m_j}{p_j} \right) \Delta_p(i).$$

Use the binomial identity (valid for $0 \leq p_i \leq m_i - 1$)

$$m_i \binom{m_i - 1}{p_i} = (m_i - p_i) \binom{m_i}{p_i},$$

to obtain

$$S_{i \rightarrow u}^{\text{LES}} = \sum_{\substack{p \in \mathcal{G}(u) \\ p_i < m_i}} \frac{|p|! (n - |p| - 1)!}{n!} \left(\prod_{j \in u} \binom{m_j}{p_j} \right) (m_i - p_i) \Delta_p(i),$$

Which is the desired result. \square

S2 Choice of \mathbf{m}

Choice of \mathbf{m} . The resolution profile $\mathbf{m} = (m_i)_{i \in u}$ controls how finely the local cube is discretized before computing within-pot attributions. Refining \mathbf{m} , micro-Shapley converges to the diagonal Aumann–Shapley / IG attribution on r_u (Theorem 2). The computational cost is governed by the grid-state evaluation $\mathcal{O}(k(m+1)^k)$ in the uniform case. On the other hand, for large total replica count $n = \sum_{j \in u} m_j$, the micro-Shapley share behaves like a Riemann sum $\frac{1}{n} \sum_{t=0}^{n-1} f_i(t/n)$ (up to a vanishing term). If f_i is L_i -Lipschitz on $[0, 1]$ (e.g., r_u is C^2 with bounded second derivatives along the diagonal), then the standard Riemann bound yields:

$$\left| \frac{1}{n} \sum_{t=0}^{n-1} f_i\left(\frac{t}{n}\right) - \int_0^1 \frac{\partial r_u}{\partial t_i}(\tau \mathbf{1}_k) d\tau \right| \leq \frac{L_i}{2n}.$$

S3 German Credit: Additional Results

	p_{logistic}	p_{mlp}	p_{xgboost}	$p_{\text{min 3}}$
Individual idx = 242	0.148	0.296	0.144	0.144

Table S1: Baseline predicted probabilities for the chosen individual (idx 242) under three models and the conservative ensemble score $p_{\text{min 3}} = \min\{p_{\text{logistic}}, p_{\text{mlp}}, p_{\text{xgboost}}\}$.

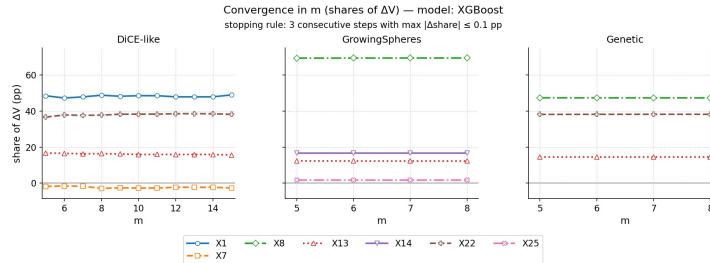


Fig. S1: m -sweep convergence (XGBoost): feature shares as a fraction of ΔV vs. grid resolution m .

DiCE-like counterfactual		$(\Delta V = 0.6993)$				
Feature	ϕ^{eq}	S^{micro}	ES	$S^{micro} - \phi^{eq}$	$S^{micro} - ES$	
X_{22} (<i>foreign_worker</i>)	0.2784	0.2964	0.2890	+0.0180	+0.0074	
X_1 (<i>Loan duration</i>)	0.2307	0.1988	0.2129	-0.0319	-0.0141	
X_{13} (<i>credit_history</i>)	0.1376	0.1774	0.1152	+0.0398	+0.0622	
X_7 (<i>telephone</i>)	0.0526	0.0268	0.0823	-0.0259	-0.0555	
Growing Spheres counterfactual		$(\Delta V = 0.6569)$				
Feature	ϕ^{eq}	S^{micro}	ES	$S^{micro} - \phi^{eq}$	$S^{micro} - ES$	
X_8 (<i>Checking Account Balance greater than 0</i>)	0.3331	0.4389	0.3013	+0.1058	+0.1376	
X_{14} (<i>Critical Account or Loans Elsewhere</i>)	0.1295	0.1130	0.1576	-0.0164	-0.0446	
X_{13} (<i>credit_history</i>)	0.1772	0.0934	0.1313	-0.0839	-0.0379	
X_{25} (<i>housing</i>)	0.0171	0.0115	0.0666	-0.0056	-0.0551	
Genetic counterfactual		$(\Delta V = 0.6941)$				
Feature	ϕ^{eq}	S^{micro}	ES	$S^{micro} - \phi^{eq}$	$S^{micro} - ES$	
X_8 (<i>Checking Account Balance greater than 0</i>)	0.3003	0.3258	0.2868	+0.0256	+0.0391	
X_{22} (<i>foreign_worker</i>)	0.2638	0.2422	0.2906	-0.0216	-0.0483	
X_{13} (<i>credit_history</i>)	0.1299	0.1260	0.1167	-0.0040	+0.0092	

Table S2: Feature-level totals (in Δ -units) under equal-split Shapley (ϕ^{eq}), TU-micro-game Shapley (S^{micro}), and Equal Surplus (ES) for the three successful counterfactuals.

Table S3: Largest within-pot reallocations between equal split and TU-micro-game Shapley for each counterfactual.

Pot T	Feature	equal	micro	$\Delta = \text{micro} - \text{equal}$
DiCE-like				
X_1 (<i>Loan duration</i>) + X_{13} (<i>credit_history</i>)	X_1	0.0622	0.0299	-0.0323
X_1 (<i>Loan duration</i>) + X_{13} (<i>credit_history</i>)	X_{13}	0.0622	0.0945	0.0323
X_{13} (<i>credit_history</i>) + X_{22} (<i>foreign_worker</i>)	X_{13}	0.0257	0.0612	0.0354
X_{13} (<i>credit_history</i>) + X_{22} (<i>foreign_worker</i>)	X_{22}	0.0257	-0.0097	-0.0354
X_1 (<i>Loan duration</i>) + X_7 (<i>telephone</i>) + X_{22} (<i>foreign_worker</i>)	X_{22}	-0.0295	0.0049	0.0344
X_1 (<i>Loan duration</i>) + X_{13} (<i>credit_history</i>) + X_{22} (<i>foreign_worker</i>)	X_{22}	-0.0324	0.0006	0.0330
Growing Spheres				
X_8 (<i>Checking Account Balance greater than 0</i>) + X_{13} (<i>credit_history</i>)	X_{13}	0.0659	0.0176	-0.0484

Table S3 (continued).

Pot T	Feature	equal	micro	$\Delta = \text{micro} - \text{equal}$
$X8(\text{Checking Account Balance greater than } 0)$	\bar{X}_8	0.0659	0.1143	0.0484
$X13(\text{credit_history})$				
$X8(\text{Checking Account Balance greater than } 0)$	\bar{X}_{14}	-0.0004	-0.0366	-0.0362
$X14(\text{Critical Account or Loans Elsewhere})$				
$X8(\text{Checking Account Balance greater than } 0)$	\bar{X}_8	-0.0004	0.0359	0.0362
$X14(\text{Critical Account or Loans Elsewhere})$				
Genetic				
$X8(\text{Checking Account Balance greater than } 0)$	\bar{X}_{13}	0.0659	0.0176	-0.0484
$X13(\text{credit_history})$				
$X8(\text{Checking Account Balance greater than } 0)$	\bar{X}_8	0.0659	0.1143	0.0484
$X13(\text{credit_history})$				
$X8(\text{Checking Account Balance greater than } 0)$	\bar{X}_{22}	0.0260	-0.0192	-0.0452
$X22(\text{foreign_worker})$				
$X8(\text{Checking Account Balance greater than } 0)$	\bar{X}_8	0.0260	0.0712	0.0452
$X22(\text{foreign_worker})$				
$X8(\text{Checking Account Balance greater than } 0)$	\bar{X}_{22}	-0.0423	0.0167	0.0590
$X13(\text{credit_history}) +$ $X22(\text{foreign_worker})$				
$X8(\text{Checking Account Balance greater than } 0)$	\bar{X}_8	-0.0423	-0.1103	-0.0680
$X13(\text{credit_history}) +$ $X22(\text{foreign_worker})$				

Table S4: Full within-pot split table for the DiCE-like counterfactual (equal split vs. TU-micro-game Shapley).

Within-pot split comparison (DiCE-like): per-feature allocations							
$ T $	ϕ_T	Pot T	$i \in T$	Eq. in pot	Micro in pot	Micro-Eq	
2	0.124,431	$X1 + X13$	$X1$	0.062,215	0.029,896	-0.032,319	
2	0.124,431	$X1 + X13$	$X13$	0.062,215	0.094,534	0.032,319	
2	0.085,342	$X1 + X22$	$X1$	0.042,671	0.035,201	-0.007,470	
2	0.085,342	$X1 + X22$	$X22$	0.042,671	0.050,141	0.007,470	
2	0.051,435	$X13 + X22$	$X13$	0.025,717	0.061,164	0.035,446	
2	0.051,435	$X13 + X22$	$X22$	0.025,717	-0.009,729	-0.035,446	
2	0.043,004	$X7 + X22$	$X22$	0.021,502	0.003,330	-0.018,172	
2	0.043,004	$X7 + X22$	$X7$	0.021,502	0.039,674	0.018,172	
2	0.022,983	$X1 + X7$	$X1$	0.011,491	0.021,925	0.010,434	
2	0.022,983	$X1 + X7$	$X7$	0.011,491	0.001,057	-0.010,434	
2	0.022,821	$X7 + X13$	$X13$	0.011,410	-0.007,625	-0.019,035	
2	0.022,821	$X7 + X13$	$X7$	0.011,410	0.030,446	0.019,035	
4	0.015,379	$X1 + X7 + X13 + X22$	$X1$	0.003,845	0.028,113	0.024,268	
4	0.015,379	$X1 + X7 + X13 + X22$	$X13$	0.003,845	-0.006,383	-0.010,227	
4	0.015,379	$X1 + X7 + X13 + X22$	$X22$	0.003,845	-0.011,486	-0.015,331	
4	0.015,379	$X1 + X7 + X13 + X22$	$X7$	0.003,845	0.005,134	0.001,289	
3	-0.017,844	$X1 + X7 + X13$	$X1$	-0.005,948	-0.011,768	-0.005,820	

Table S4 (continued).

$ T $	ϕ_T	Pot T	$i \in T$	Eq. in pot	Micro in pot	Micro-Eq
3	-0.017,844	$X1 + X7 + X13$	X13	-0.005,948	0.013,143	0.019,091
3	-0.017,844	$X1 + X7 + X13$	X7	-0.005,948	-0.019,219	-0.013,271
3	-0.023,743	$X7 + X13 + X22$	X13	-0.007,914	0.001,907	0.009,822
3	-0.023,743	$X7 + X13 + X22$	X22	-0.007,914	0.004,164	0.012,078
3	-0.023,743	$X7 + X13 + X22$	X7	-0.007,914	-0.029,814	-0.021,900
3	-0.088,441	$X1 + X7 + X22$	X1	-0.029,480	-0.045,140	-0.015,660
3	-0.088,441	$X1 + X7 + X22$	X22	-0.029,480	0.004,948	0.034,428
3	-0.088,441	$X1 + X7 + X22$	X7	-0.029,480	-0.048,249	-0.018,768
3	-0.097,196	$X1 + X13 + X22$	X1	-0.032,399	-0.037,766	-0.005,367
3	-0.097,196	$X1 + X13 + X22$	X13	-0.032,399	-0.060,007	-0.027,609
3	-0.097,196	$X1 + X13 + X22$	X22	-0.032,399	0.000,577	0.032,976

Table S5: Full within-pot split table for the Growing Spheres counterfactual (equal split vs. TU-micro-game Shapley).

Within-pot split comparison (Growing Spheres): per-feature allocations						
$ T $	ϕ_T	Pot T	$i \in T$	Eq. in pot	Micro in pot	Micro-Eq
2	0.131,875	$X8 + X13$	X13	0.065,937	0.017,550	-0.048,387
2	0.131,875	$X8 + X13$	X8	0.065,937	0.114,324	0.048,387
3	0.072,699	$X8 + X13 + X25$	X13	0.024,233	0.009,205	-0.015,028
3	0.072,699	$X8 + X13 + X25$	X25	0.024,233	0.012,196	-0.012,038
3	0.072,699	$X8 + X13 + X25$	X8	0.024,233	0.051,299	0.027,066
3	0.033,665	$X8 + X13 + X14$	X13	0.011,222	0.010,146	-0.001,076
3	0.033,665	$X8 + X13 + X14$	X14	0.011,222	-0.000,047	-0.011,269
3	0.033,665	$X8 + X13 + X14$	X8	0.011,222	0.023,566	0.012,345
2	0.023,222	$X13 + X14$	X13	0.011,611	-0.016,968	-0.028,579
2	0.023,222	$X13 + X14$	X14	0.011,611	0.040,190	0.028,579
3	0.018,269	$X8 + X14 + X25$	X14	0.006,090	0.005,801	-0.000,289
3	0.018,269	$X8 + X14 + X25$	X25	0.006,090	0.006,446	0.000,356
3	0.018,269	$X8 + X14 + X25$	X8	0.006,090	0.006,023	-0.000,067
2	0.008,074	$X14 + X25$	X14	0.004,037	0.004,037	0.000,000
2	0.008,074	$X14 + X25$	X25	0.004,037	0.004,037	0.000,000
2	-0.000,702	$X8 + X14$	X14	-0.000,351	-0.036,585	-0.036,235
2	-0.000,702	$X8 + X14$	X8	-0.000,351	0.035,884	0.036,235
3	-0.007,007	$X13 + X14 + X25$	X13	-0.002,336	0.007,769	0.010,105
3	-0.007,007	$X13 + X14 + X25$	X14	-0.002,336	-0.005,756	-0.003,420
3	-0.007,007	$X13 + X14 + X25$	X25	-0.002,336	-0.009,020	-0.006,684
2	-0.012,562	$X13 + X25$	X13	-0.006,281	-0.009,245	-0.002,964
2	-0.012,562	$X13 + X25$	X25	-0.006,281	-0.003,317	0.002,964
4	-0.031,142	$X8 + X13 + X14 + X25$	X13	-0.007,785	-0.005,709	0.002,077
4	-0.031,142	$X8 + X13 + X14 + X25$	X14	-0.007,785	-0.001,576	0.006,209
4	-0.031,142	$X8 + X13 + X14 + X25$	X25	-0.007,785	-0.001,654	0.006,132
4	-0.031,142	$X8 + X13 + X14 + X25$	X8	-0.007,785	-0.022,203	-0.014,418
2	-0.033,785	$X8 + X25$	X25	-0.016,893	-0.013,184	0.003,709
2	-0.033,785	$X8 + X25$	X8	-0.016,893	-0.020,601	-0.003,709

Within-pot split comparison (Genetic): per-feature allocations						
$ T $	ϕ_T	Pot T	$i \in T$	Eq. in pot	Micro in pot	Micro-Eq
2	0.131,875	X8 + X13	X13	0.065,937	0.017,550	-0.048,387
2	0.131,875	X8 + X13	X8	0.065,937	0.114,324	0.048,387
2	0.052,035	X8 + X22	X22	0.026,018	-0.019,158	-0.045,175
2	0.052,035	X8 + X22	X8	0.026,018	0.071,193	0.045,175
2	0.051,435	X13 + X22	X13	0.025,717	0.061,164	0.035,446
2	0.051,435	X13 + X22	X22	0.025,717	-0.009,729	-0.035,446
3	-0.127,045	X8 + X13 + X22	X13	-0.042,348	-0.033,386	0.008,962
3	-0.127,045	X8 + X13 + X22	X22	-0.042,348	0.016,676	0.059,024
3	-0.127,045	X8 + X13 + X22	X8	-0.042,348	-0.110,335	-0.067,986

Table S6: Full within-pot split table for the Genetic counterfactual (equal split vs. TU-micro-game Shapley).

S4 MNIST: Additional Results

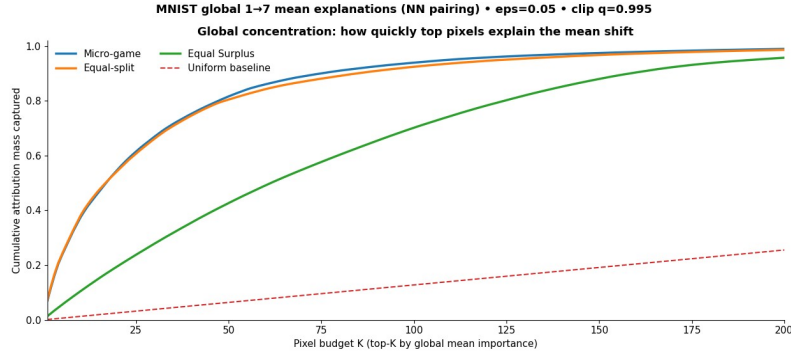


Fig. S2: Global Concentration: how quickly top pixels explain the mean shift

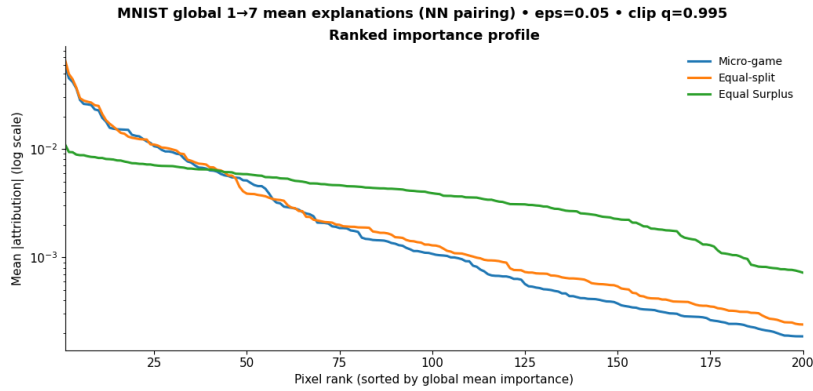


Fig. S3: Ranked importance profile

Global (dataset-level) averages — All features (n=144/144, $\bar{k} = 2.51$, <i>fallback</i> = 0.078)					
Feature	$\overline{\phi^{\text{eq}}}$	$\overline{S^{\text{micro}}}$	\overline{ES}	$\overline{S^{\text{micro}} - \phi^{\text{eq}}}$	$\overline{S^{\text{micro}} - ES}$
X2 (<i>amount (credit amount)</i>)	0.2370	0.2255	0.2295	-0.0116	-0.0040
X1 (<i>duration (months)</i>)	0.2103	0.2195	0.2028	+0.0092	+0.0167
X8 (<i>checking</i>)	0.0755	0.0767	0.0755	+0.0012	+0.0011
X24 (<i>age</i>)	0.0437	0.0425	0.0450	-0.0012	-0.0025
X22 (<i>foreign_worker</i>)	0.0229	0.0223	0.0233	-0.0006	-0.0010
X13 (<i>credit_history</i>)	0.0216	0.0199	0.0206	-0.0017	-0.0007
X17 (<i>other_debtors</i>)	0.0159	0.0173	0.0161	+0.0014	+0.0012
X14 (<i>credit_history</i>)	0.0103	0.0120	0.0100	+0.0017	+0.0020
X4 (<i>residence (years at current address)</i>)	0.0087	0.0092	0.0109	+0.0005	-0.0017
X11 (<i>savings</i>)	0.0045	0.0045	0.0054	+0.0001	-0.0008
X25 (<i>housing</i>)	0.0037	0.0041	0.0039	+0.0004	+0.0002
X19 (<i>employment</i>)	0.0031	0.0034	0.0034	+0.0003	-0.0000
X18 (<i>employment</i>)	0.0025	0.0027	0.0028	+0.0002	-0.0001
X7 (<i>telephone</i>)	0.0021	0.0026	0.0021	+0.0004	+0.0004
X12 (<i>credit_history</i>)	0.0021	0.0024	0.0019	+0.0003	+0.0005
X20 (<i>employment</i>)	0.0018	0.0021	0.0020	+0.0003	+0.0001
X15 (<i>other_plans</i>)	0.0030	0.0019	0.0026	-0.0011	-0.0007
X3 (<i>installment_rate</i>)	0.0016	0.0016	0.0020	-0.0000	-0.0005
X21 (<i>personal_status_sex</i>)	0.0008	0.0009	0.0013	+0.0002	-0.0004
X6 (<i>liable_people</i>)	0.0004	0.0005	0.0020	+0.0000	-0.0015
X27 (<i>job</i>)	0.0002	0.0003	0.0024	+0.0001	-0.0021
X23 (<i>personal_status_sex</i>)	0.0001	0.0003	0.0002	+0.0002	+0.0001
X26 (<i>housing</i>)	-0.0002	-0.0002	0.0014	+0.0000	-0.0016
X10 (<i>savings in {A62,A63,A64}</i>)	0.0001	-0.0000	0.0005	-0.0001	-0.0006
X16 (<i>other_debtors</i>)	0.0000	-0.0000	0.0021	-0.0001	-0.0022
X5 (<i>existing_credits</i>)	0.0001	-0.0000	0.0021	-0.0001	-0.0021
X9 (<i>checking</i>)	0.0000	0.0000	0.0000	0.0000	0.0000

Table S7: Dataset-level average feature totals under equal splitting (ϕ^{eq}), grid-state TU-micro-game Shapley (S^{micro}), and Equal Surplus (ES), reported for all features. (Fitted on XGBoost/DiCE).

Bibliography

- [1] Apley, D.W., Zhu, J.: Visualizing the effects of predictor variables in black box supervised learning models. *J. R. Stat. Soc. Ser. B* **82**(4) (2020)
- [2] Aumann, R.J., Shapley, L.S.: *Values of Non-Atomic Games*. Princeton Univ. Press (1974)
- [3] Béal, S., Rémila, E., Solal, P.: Decomposition of the space of TU-games, strong transfer invariance and the Banzhaf value. *Oper. Res. Lett.* **43**(2), 123–125 (2015)
- [4] Breiman, L.: Random forests. *Mach. Learn.* **45**(1), 5–32 (2001)
- [5] Chameni Nembua, C.: Linear efficient and symmetric values for TU-games: Sharing the joint gain of cooperation. *Games Econ. Behav.* **74**(1) (2012)
- [6] Chameni Nembua, C., Andjiga, N.G.: Linear, efficient and symmetric values for TU-games. *Econ. Bull.* **3**(71), 1–10 (2008)
- [7] Condevaux, C., Harispe, S., Mussard, S.: Fair and efficient alternatives to shapley-based attribution methods. In: *Machine Learning and Knowledge Discovery in Databases (ECML PKDD 2022)*, Proceedings, Part I. Lecture Notes in Computer Science, vol. 13713, pp. 309–324. Springer (2022)
- [8] De Bock, K.W., Coussement, K., De Caigny, A., Słowiński, R., Baesens, B., Boute, R.N., Choi, T.M., Delen, D., Kraus, M., Lessmann, S., Maldonado, S., Martens, D., Óskarsdóttir, M., Vairetti, C., Verbeke, W., Weber, R.: Explainable AI for operational research: A defining framework, methods, applications, and a research agenda. *Eur. J. Oper. Res.* **317**(2) (2024)
- [9] Friedman, J.H.: Greedy function approximation: A gradient boosting machine. *Ann. Stat.* **29**(5), 1189–1232 (2001)
- [10] Frye, C., Rowat, I., Feige, I.: Asymmetric shapley values: Incorporating causal knowledge into model-agnostic explainability. In: *NeurIPS*. vol. 33, pp. 13963–13973 (2020)
- [11] Goldstein, A., Kapelner, A., Bleich, J., Pitkin, E.: Peeking inside the black box: Visualizing statistical learning with plots of individual conditional expectation. *J. Comput. Graph. Stat.* **24**(1), 44–65 (2015)
- [12] Harsanyi, J.C.: A simplified bargaining model for the n -person cooperative game. *Int. Econ. Rev.* **4**(2), 194–220 (1963)
- [13] He, K., Zhang, X., Ren, S., Sun, J.: Deep residual learning for image recognition. In: *Proc. CVPR*. pp. 770–778 (2016)
- [14] Heskes, T., Sijben, E., Bucur, I.A., Claassen, T.: Causal shapley values: Exploiting causal knowledge to explain individual predictions of complex models. In: *NeurIPS*. vol. 33, pp. 9698–9708 (2020)
- [15] Hofmann, H.: *Statlog (german credit data)* (1994), uCI ML Repository
- [16] Karimi, A.H., Schölkopf, B., Valera, I.: Algorithmic recourse: From counterfactual explanations to interventions. In: *Proc. FAccT*. pp. 353–362 (2021)
- [17] Laugel, T., Lesot, M.J., Marsala, C., Renard, X., Detyniecki, M.: Comparison-based inverse classification for interpretability in machine learning. In: *IPMU*. vol. 853, pp. 100–111. Springer, Cham (2018)

- [18] LeCun, Y., Cortes, C., Burges, C.J.C.: Mnist handwritten digit database (2010), online
- [19] Lu, X., Borgonovo, E.: Unveiling the path to desired predictions: An interpretability approach for black-box models. In: SIAM UQ (2024)
- [20] Lundberg, S.M., Lee, S.: A unified approach to interpreting model predictions. In: NeurIPS, vol. 30, pp. 4765–4774. Curran Assoc. (2017)
- [21] Mothilal, R.K., Sharma, A., Tan, C.: Explaining machine learning classifiers through diverse counterfactual explanations. In: Proceedings of the 2020 Conference on Fairness, Accountability, and Transparency (FAT* '20). pp. 607–617. ACM (2020)
- [22] Radzik, T., Driessen, T.: On a family of values for TU-games generalizing the Shapley value. *Math. Soc. Sci.* **65**(2), 105–111 (2013)
- [23] Ribeiro, M.T., Singh, S., Guestrin, C.: “why should i trust you?”: Explaining the predictions of any classifier. In: Proc. KDD. pp. 1135–1144 (2016)
- [24] Ruiz, L.M., Valenciano, F., Zarzuelo, J.M.: The family of least square values for transferable utility games. *Games Econ. Behav.* **24**(1–2), 109–130 (1998)
- [25] Selvaraju, R.R., Cogswell, M., Das, A., Vedantam, R., Parikh, D., Batra, D.: Grad-CAM: Visual explanations from deep networks via gradient-based localization. In: Proc. ICCV. pp. 618–626 (2017)
- [26] Shapley, L.S.: A value for n -person games. In: Kuhn, H.W., Tucker, A.W. (eds.) *Contrib. Theory Games II*, *Ann. Math. Stud.*, vol. 28, pp. 307–317. Princeton Univ. Press (1953)
- [27] Shi, Y., Peng, T., Pan, Q.: Bank financial sustainability evaluation: A network DEA-SHAP analysis. *Eur. J. Oper. Res.* **321**, 614–630 (2025)
- [28] Smilkov, D., Thorat, N., Kim, B., Viégas, F., Wattenberg, M.: Smoothgrad: Removing noise by adding noise. In: Workshop on Visualization for Deep Learning, ICML 2017 (2017), workshop paper
- [29] Sobol’, I.M.: Sensitivity Estimates for Nonlinear Mathematical Models. *Math. Model. Comput. Exp.* (1993)
- [30] Sundararajan, M., Dhamdhere, K., Agarwal, A.: The shapley taylor interaction index. In: Proceedings of the 37th International Conference on Machine Learning. Proceedings of Machine Learning Research, vol. 119, pp. 9259–9268. PMLR (2020)
- [31] Sundararajan, M., Najmi, A.: The many shapley values for model explanation. In: Proc. ICML. Proc. Mach. Learn. Res., vol. 119, pp. 9269–9278. PMLR (2020)
- [32] Sundararajan, M., Taly, A., Yan, Q.: Axiomatic attribution for deep networks. In: Proc. ICML. Proc. Mach. Learn. Res., vol. 70 (2017)
- [33] Ustun, B., Spangher, A., Liu, Y.: Actionable recourse in linear classification. In: Proc. FAT*. pp. 10–19 (2019)
- [34] Verma, S., Boonsanong, V., Hoang, M., Hines, K.E., Dickerson, J.P., Shah, C.: Counterfactual explanations and algorithmic recourses for machine learning: A review. *ACM Comput. Surv.* **56**(12), 1–42 (2024)
- [35] Wachter, S., Mittelstadt, B., Russell, C.: Counterfactual explanations without opening the black box: Automated decisions and the gdpr. *Harvard Journal of Law & Technology* **31**(2), 841–887 (2018)